

**Electronic, vibrational, and optical properties of fullerene-S₈ co-crystals**

Journal:	<i>Journal of Materials Chemistry C</i>
Manuscript ID	TC-ART-09-2023-003358.R1
Article Type:	Paper
Date Submitted by the Author:	09-Nov-2023
Complete List of Authors:	Shaban Tameh, Maliheh; The University of Arizona, Chemistry and Biochemistry Ni, Xiaojuan; The University of Arizona, Chemistry and Biochemistry Bredas, Jean-Luc ; The University of Arizona, Chemistry and Biochemistry Coropceanu, Veaceslav; The University of Arizona, Chemistry and Biochemistry

Electronic, vibrational, and optical properties of fullerene-S₈ co-crystals [#]

Maliheh Shaban Tameh, Xiaojuan Ni,

Veaceslav Coropceanu,^{*} and Jean-Luc Brédas^{*}

Department of Chemistry and Biochemistry

The University of Arizona

Tucson, Arizona 85721-0041

* Emails: coropceanu@arizona.edu; jlbredas@arizona.edu

[#] This work is dedicated to the memory of Professor Gilles Horowitz, a pioneer of the field of organic electronics, a gentleman, and a mentor who inspired generations of scientists.

Abstract

Sulfur and fullerenes are well-known materials that have received significant attention over many years and fullerene-S₈ co-crystals have been reported recently. Here, via density functional theory (DFT) calculations, we shed light on the electronic, vibrational, and optical properties of the C₆₀-2S₈ and C₇₀-2S₈ co-crystals. In both co-crystals, the holes and electrons are characterized by very small effective masses that are comparable to those derived in fullerene single crystals. Interestingly, the S₈ molecules are found not to contribute to charge transport as the calculations show that both types of carriers move over the networks formed by the fullerene molecules. Calculations of the excited electronic states point to the formation of charge-transfer states, where electrons are transferred from fullerene molecules to S₈ molecules, *i.e.*, the fullerenes act in these co-crystals as electron donors. However, the energies of these charge-transfer states in both C₆₀-2S₈ and C₇₀-2S₈ are higher than those of several excited states localized on C₆₀ or C₇₀; therefore, the charge-transfer states play no role in the low-energy part of the absorption spectrum. In agreement with experimental data, the calculations also show that the fullerene-S₈ intermolecular interactions are very weak in the ground state; as a result, the infrared (IR) spectra of the co-crystals represent a simple superposition of the spectra of S₈ and fullerene molecules. Since the spectra are largely silent in the long-wave IR region (800-1250 cm⁻¹), these fullerene-S₈ co-crystals are potential candidates for thermal IR imaging applications.

1. Introduction

Sulfur, especially as a by-product of oil refinery, is an inexpensive and abundant material that is attracting a great deal of attention. For instance, polymers with a high sulfur content are currently used in a broad range of applications¹⁻¹² including thermal IR imaging,^{1, 2} Li-S batteries,^{3, 4} repairable materials,^{5, 6} and environmental remediation.⁷ Elemental sulfur can be found in a variety of allotropes,¹³⁻¹⁷ with the crown-shaped S₈ ring being thermodynamically the most stable form in the normal state.¹⁸⁻²⁰ S₈-ring molecules form the basis for the crystal structure stable at room temperature, which is transparent in the visible.^{21, 22} In addition, there are many examples of compounds in which S₈ has been co-crystallized with a range of other molecules.²³⁻³⁶

The C₆₀ and C₇₀ buckminsterfullerenes also consist of a single chemical element, in this case carbon. C₆₀ and C₇₀ and their derivatives have had a significant impact on a broad range of applications ranging from solar cells to hydrogen gas storage, field-effect transistors, and photodetectors.³⁷⁻⁴³ Fullerenes have been exploited as both electron donating and electron accepting materials and have been shown to display ambipolar charge transport with equivalent hole and electron mobilities.⁴⁴⁻⁴⁹

One of the first studies related to fullerene-sulfur interactions was based on C₆₀ films doped with sulfur.⁵⁰ The electrical conductivity of these doped films was found to increase by many orders of magnitude at high temperature, which was attributed to a donating nature of sulfur. Co-crystals containing the C₆₀ or C₇₀ fullerene and S₈ rings have also been of interest for many years. These systems were developed, in particular, with the hope to achieve covalent or donor-acceptor interactions between the fullerene molecules and the sulfur rings. For example, C₆₀ – 2S₈, C₇₀ – 2

S_8 , $C_{70} - S_8$, and $C_{70} - 6S_8$ co-crystals have been synthesized and investigated.^{25,26,51-59} In contrast to the sulfur-doped C_{60} films, the conductivity measurements on these co-crystals have shown they are insulators or semiconductors.⁵⁸ Very recently, it was demonstrated that $C_{60} - 2S_8$ co-crystals could be used to develop cathode materials for high-performance Li-S batteries.⁶⁰ Fullerene- S_8 co-crystals have also received interest with regard to the evolution of their electronic properties under high-pressure conditions.⁶¹

In spite of the broad interest raised by fullerene- S_8 co-crystals, a detailed description of the nature of the fullerene-sulfur interactions and of their impact on the system electronic properties remains missing. In this work, we use density functional theory (DFT) calculations to shed light on the charge transport, vibrational, and optical properties of the $C_{70} - 2S_8$ and $C_{60} - 2S_8$ co-crystals.^{25, 52, 59}

2. Computational Methodology

Density functional theory (DFT) calculations on the periodic structures of the $C_{60} - 2S_8$ and $C_{70} - 2S_8$ co-crystals were carried out using the projector-augmented wave method as implemented in the Vienna ab initio simulation package (VASP),⁶²⁻⁶⁴ with the Perdew-Burke-Ernzerhof (PBE) functional and considering a Pack-Monkhorst Γ -centered k-point mesh of $2 \times 2 \times 2$. The crystal structures were optimized by relaxing the atomic coordinates until the total force on each atom was less than $0.01 \text{ eV}/\text{\AA}$. Band structures and gamma-point phonon calculations were performed at the same level of theory. The infrared absorption intensities were calculated using the density functional perturbation theory approach.^{65,66} The effective masses at the valence band maxima and

conduction band minima were calculated through diagonalizing the (m_{ij}^{-1}) tensor using a finite difference method on a five-point stencil with a 0.01 Bohr⁻¹ step:

$$\frac{1}{m_{ij}} = \frac{1}{\hbar^2} \frac{\partial^2 E}{\partial k_i \partial k_j} \quad (1)$$

The hole and electron transfer integrals between adjacent molecules in the crystal were derived using a fragment orbital approach in combination with a basis set orthogonalization procedure.⁶⁷ ⁶⁸ These calculations were performed using the PBE and B3LYP functionals with the 6-31G (d,p) basis set. The same level of theory was also used to derive the IR vibrational spectra of the C₆₀ and C₇₀ molecules. In addition, time-dependent (TD) DFT calculations at the B3LYP/6-31G (d,p) and long-range corrected LC- ω HPBE/6-31G (d,p) levels were performed to calculate the excited-state energies of C₇₀-S₈ and C₇₀-S₈ complexes extracted from the crystal structures. In the case of the LC- ω HPBE functional, the range-separation parameter, ω , was tuned for each system following the procedure reported earlier⁶⁹; ω values of 0.49, 0.47, and 0.49 bohr⁻¹ were optimized for C₆₀, C₇₀, and S₈, respectively. We considered 20% of Hartree-Fock exchange in the short range and a dielectric constant $\epsilon = 4$, which is appropriate for both S₈ and fullerene systems.^{70, 71} All electronic-structure calculations on isolated molecules and molecular complexes were performed with the Gaussian 16 package.⁷²

3. Results and Discussion

Electronic structure. There are four known polymorph forms of the C₆₀–2S₈ co-crystal.²⁵ We focus here on the β -polymorph as it does not display any disorder of the C₆₀ cages (hereafter, we

refer to this polymorph simply as $C_{60}-2S_8$). $C_{60}-2S_8$ has a $P\bar{1}$ triclinic structure while $C_{70}-2S_8$ belongs to the $P2_1/C$ monoclinic space group.⁵² The asymmetric units of both co-crystals consist of two fullerene and four S_8 translationally inequivalent molecules. In both co-crystals, the S_8 and fullerene molecules pack in adjacent segregated stacks, see Figure 1. The molecular stacking is along the a axis in the case of $C_{60}-2S_8$ and along the c axis in the case of $C_{70}-2S_8$. Importantly, the intermolecular center-to-center distances between fullerene molecules are just above 1 nm, *i.e.*, twice the van der Waals radius of the fullerenes, which points to the possibility of large electronic interactions among C_{60} and C_{70} molecules in these co-crystals.

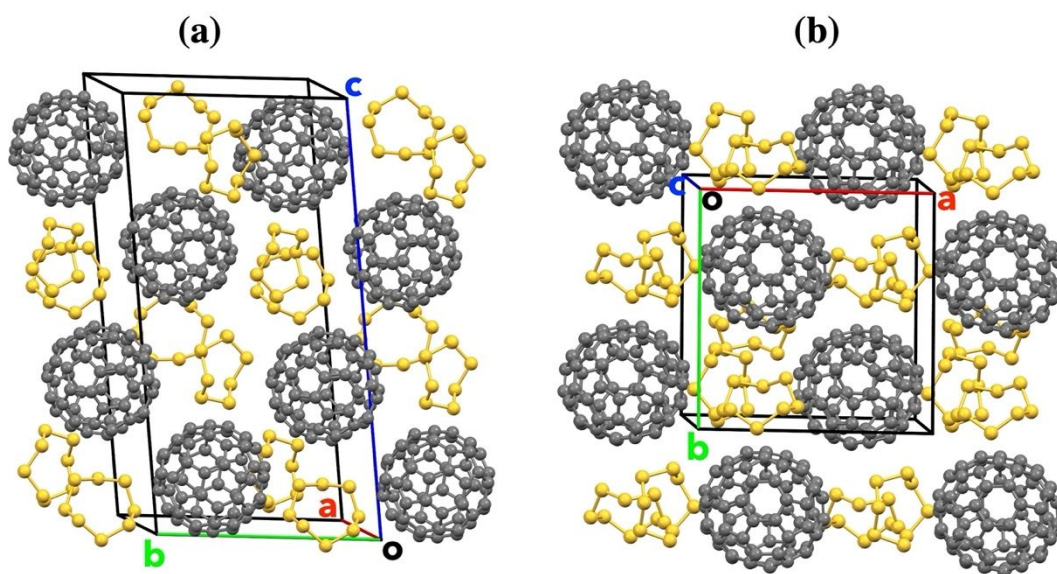


Figure 1. Schematic representation of the crystal structures of $C_{60}-2S_8$ (a) and $C_{70}-2S_8$ (b).

The band structures of the $C_{60}-2S_8$ and $C_{70}-2S_8$ co-crystals obtained at the PBE/6-31G (d,p) level are shown in **Figure 2**. The results indicate that the top of valence band (VB) and the bottom of the conduction band (CB) in both co-crystals are dominated by the fullerene wavefunctions. To understand this feature, we computed the energies of the C_{60} and C_{70} frontier orbitals using the

same molecular geometries as those in the periodic band structure calculations. As seen from **Table 1**, the S_8 HOMO level is located about 0.7 eV lower than those of the C_{60} and C_{70} molecules while the S_8 LUMO is found about 0.5 eV above the LUMO levels of the fullerenes. The calculations performed at the B3LYP/6-31G(d,p) and LC- ω HPBE/6-31G (d,p) levels also support this conclusion (see **Table 1**). We note that, here, we are interested in the *relative* positions of the frontier molecular levels rather than in their actual energies (which clearly depend on the choice of the functional, as seen from Table 1). The DFT calculations indicate that the electronic couplings between the S_8 and fullerene frontier orbitals (see **Tables S1-S2** in the supplemental information (SI)) do not exceed 100 meV, which points to only minor hybridization between fullerene and S_8 levels.

In the case of $C_{60} - 2S_8$, the VB maximum is located at $\Delta_L = (0.5, -0.429, 0)$, *i.e.*, close to high-symmetry point L = (0.5, -0.5, 0). As seen from **Figure 2**, there is no significant band dispersion along YL and ZN, which means that there are only weak interactions between C_{60} fullerenes along the *b*-axis in real space. In contrast, the valence band is more dispersive along the ΓY , $L\Gamma$, and ΓZ *k*-paths, demonstrating significant coupling among C_{60} frontier orbitals along the *a*-axis, *i.e.*, along the stacking direction of the C_{60} molecules. This finding is consistent with the results obtained for the effective masses, see **Table 2**. The smallest effective hole mass, about $\sim 1 m_0$ (where m_0 is the electron mass at rest) is found indeed along the *a*-axis and the largest hole mass component (61 m_0) is found along the *b*-axis. Additional direct calculations of the transfer integrals confirm that there exists a significant electronic coupling (33 meV) along the *a*-axis direction (see **Figure S1** and **Table S3**).

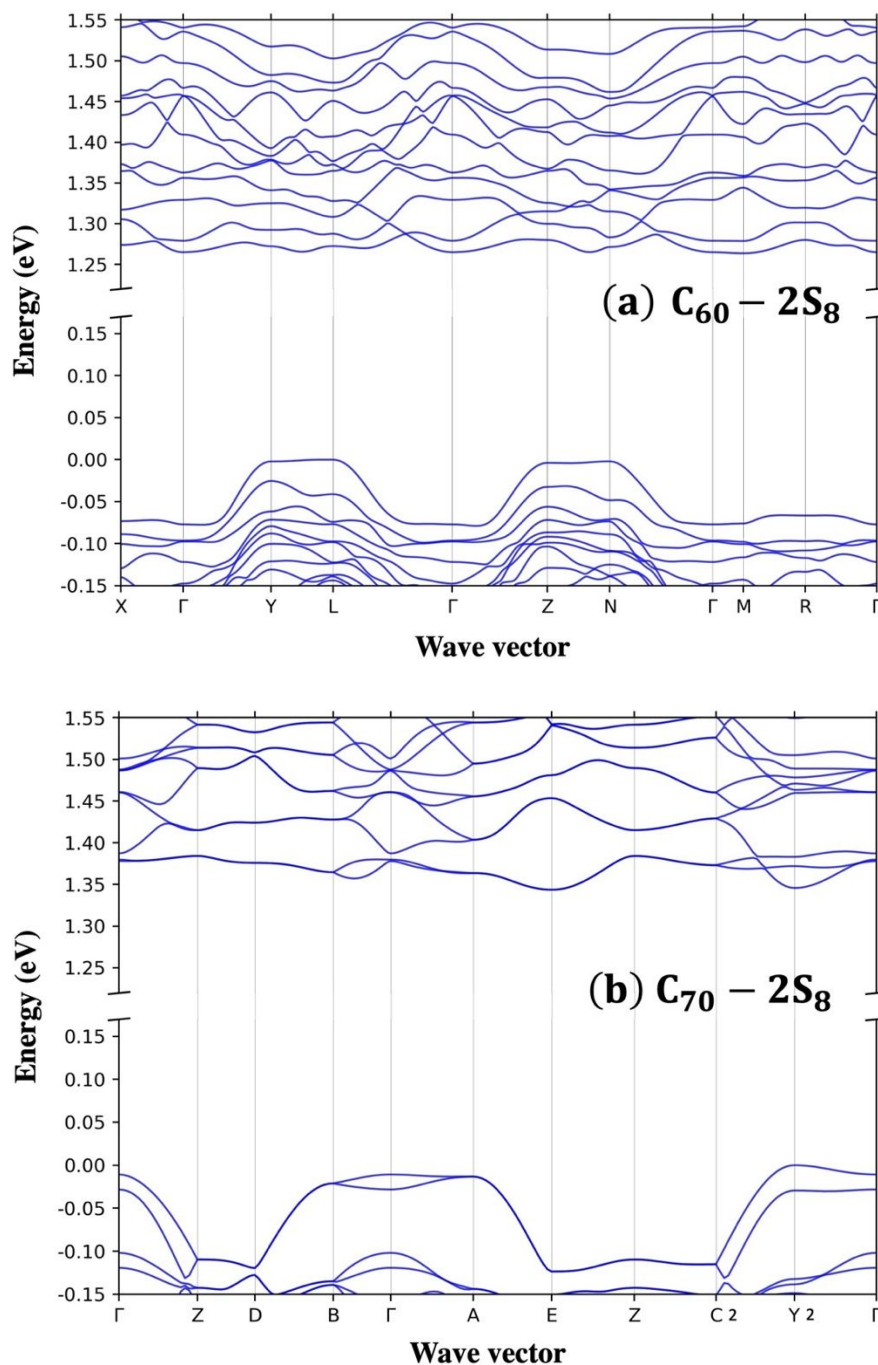


Figure 2. (a) Electronic band structure of $C_{60} - 2S_8$. The points of high symmetry in the first Brillouin zone are labeled as follows: $X = (0, -0.5, 0)$, $\Gamma = (0, 0, 0)$, $Y = (0.5, 0, 0)$, $L = (0.5, -0.5, 0)$, $\Gamma = (0, 0, 0)$, and $Z = (-0.5, 0, 0.5)$, $N = (-0.5, -0.5, 0.5)$, $\Gamma = (0, 0, 0)$, $M = (0, 0, 0.5)$, $R = (0, -0.5, 0.5)$, $\Gamma = (0, 0, 0)$. (b) Electronic band structure of $C_{70} - 2S_8$. The points of high symmetry in the first Brillouin zone are labeled as follows: $\Gamma = (0, 0, 0)$, $Z = (0, 0.5, 0)$, $D = (0, 0.5, 0.5)$, $B = (0, 0, 0.5)$, $\Gamma =$

(0,0,0), $A = (-0.5,0,0.5)$, $E = (-0.5,0.5,0.5)$, $Z = (0,0.5,0)$, $C_2 = (-0.5,0.5,0)$, $Y_2 = (-0.5,0,0)$, and $\Gamma = (0,0,0)$. All points are given in fractional coordinates in reciprocal space. The zero of energy is taken as the top of the VB.

Table 1. Frontier orbital energies (in eV) of C_{60} , C_{70} , and S_8 , as calculated at the B3LYP/6-31G (d,p), PBE/6-31G (d,p), and LC- ω HPBE/6-31G (d,p) levels of theory.

Molecule	B3LYP		PBE		LC- ω HPBE	
	HOMO	LUMO	HOMO	LUMO	HOMO	LUMO
C_{60}	-5.99	-3.23	-5.50	-3.83	-6.30	-3.28
C_{70}	-5.91	-3.25	-5.48	-3.75	-6.23	-3.30
S_8	-6.66	-2.59	-6.62	-3.29	-7.75	-2.59

The bottom of the CB in $C_{60} - 2S_8$ has several local minima [*i.e.*, $\Delta_\Gamma = (-0.007, -0.003, 0.010)$, $\Delta_N = (-0.531, -0.357, 0.578)$, and $\Delta_M = (-0.007, -0.003, 0.010)$] with nearly identical energies (within 3 meV). The largest band dispersion is observed along the ΓL , ΓN , and ΓX pathways. This results into two small effective-mass components of $1m_0$ and $1.7 m_0$ along the b -axis and in the ac plane, respectively. Thus, in the case of electrons, charge transport in the $C_{60} - 2S_8$ co-crystal has more of a 3D character. For the sake of comparison, we note that the effective masses for holes and electrons in the face-centered-cubic C_{60} crystal are $1.7 m_0$ and $1.3 m_0$, respectively.⁷³

The $C_{70} - 2S_8$ band structure is depicted in **Figure 2b**. We note that, in this co-crystal, the C_{70} molecules stack along the c -axis. The maximum of the VB is located at $Y_2 = (-0.5,0,0)$. The top of the VB displays moderate band dispersion along the ZC_2 , $Y_2\Gamma$, ZD , and EZ k-paths, suggesting weak interactions among C_{70} molecules along the a -axis and c -axis in real space. However, significant dispersion is observed along the Y_2C_2 and AE directions, *i.e.*, along the b -axis. The effective-mass calculations show that the smallest component for holes ($1.7 m_0$) is oriented indeed

along the b -axis. The CB minimum is located at $E = (-0.5, 0.5, 0.5)$. As in the case of $C_{60}-2S_8$, the CB also displays an additional local minimum at $Y_2 = (-0.5, 0, 0)$, located just 2 meV above the E point. As for the holes, the smallest effective-mass component for electrons ($1 m_0$) is obtained along the b -axis. However, relatively small effective-mass values ($< 2 m_0$) are also obtained for electrons moving in the ac plane, suggesting that, as in the case of $C_{60}-2S_8$, the electrons in $C_{70}-2S_8$ display a 3D charge transport character.

Table 2. Hole and electron effective masses m (in units of the electron mass at rest, m_0) at the band extrema of $C_{60}-2S_8$ and $C_{70}-2S_8$.

		m/m_0	Parallel to
$C_{60} - 2S_8$	Holes at Δ_L	1.0	$\mathbf{a} - 0.040\mathbf{b} - 0.011\mathbf{c}$
		61.0	$0.041\mathbf{a} + \mathbf{b} + 0.080\mathbf{c}$
		6.6	$0.007\mathbf{a} - 0.080\mathbf{b} + \mathbf{c}$
	Electrons at Δ_Γ	1.7	$0.722\mathbf{a} - 0.293\mathbf{b} + 0.626\mathbf{c}$
		1.0	$0.246\mathbf{a} + 0.956\mathbf{b} + 0.163\mathbf{c}$
		4.8	$-0.646\mathbf{a} + 0.036\mathbf{b} + 0.762\mathbf{c}$
$C_{70} - 2S_8$	Holes at Y_2	5.4	$0.815\mathbf{a} + 0.579\mathbf{c}$
		1.1	\mathbf{b}
		16.3	$-0.579\mathbf{a} + 0.815\mathbf{c}$
	Electrons at Y_2	2.416	$\mathbf{a} + 0.142\mathbf{c}$
		0.956	\mathbf{b}
		4.464	$-0.142\mathbf{a} + \mathbf{c}$
		3.520	$0.997\mathbf{a} - 0.005\mathbf{b} + 0.077\mathbf{c}$
		Electrons at E	3.271
	1.681	$-0.077\mathbf{a} + 0.004\mathbf{b} + 0.997\mathbf{c}$	

Infrared (IR) properties. As mentioned in the Introduction, polymers with a high sulfur content have emerged as a new class of materials for IR imaging.^{1, 74-76} Regions of special interest are the long-wave (LWIR, 8-12.5 μm / 800-1250 cm^{-1}) and mid-wave (MWIR, 3-5 μm / 2000-3300 cm^{-1}) IR spectral windows.¹ Experimental data show that S_8 exhibits only a few weak IR transitions that are found in the range of 100-500 cm^{-1} .⁷⁷ Thus, S_8 is transparent in both LWIR and MWIR windows. In a recent theoretical work, we showed that the C_{60} and C_{70} molecules are also fully transparent in the MWIR window and highly transparent in the LWIR region.⁷⁸ Therefore, it is

interesting to investigate the evolution of the IR properties when considering fullerene-S₈ co-crystals.

The PBE IR spectra of C₆₀-2S₈ and C₇₀-2S₈ co-crystals along with those of the isolated C₆₀ and C₇₀ molecules are displayed in **Figure 3**. We note that the PBE/6-31G(d,p) and B3LYP/6-31G(d,p) calculations yield similar results for the investigated systems, as shown in **Figures S2** and **S3**. As illustrated in **Figure 3**, the IR spectra of both C₆₀-2S₈ and C₇₀-2S₈ co-crystals resemble very closely the spectra of C₆₀ and C₇₀ molecules, respectively. Some doublings of the peaks seen at high energies in Figure 3 are due to the presence of translationally inequivalent fullerene molecules in the unit cell. Overall, the IR results are consistent with the fact that there is only negligible charge transfer between fullerene and S₈ molecules in the ground state and that the intermolecular interactions are entirely driven by weak van der Waals forces. This conclusion is also supported by experimental data^{58, 59} showing that the IR spectra of the C₆₀-2S₈ and C₇₀-2S₈ films are very similar to the spectra of the related fullerene molecules. Thus, we expect that the C₆₀-2S₈ and C₇₀-2S₈ co-crystals, as is the case for the C₆₀ and C₇₀ films, are potential candidates as IR imaging materials in both LWIR and MWIR windows.

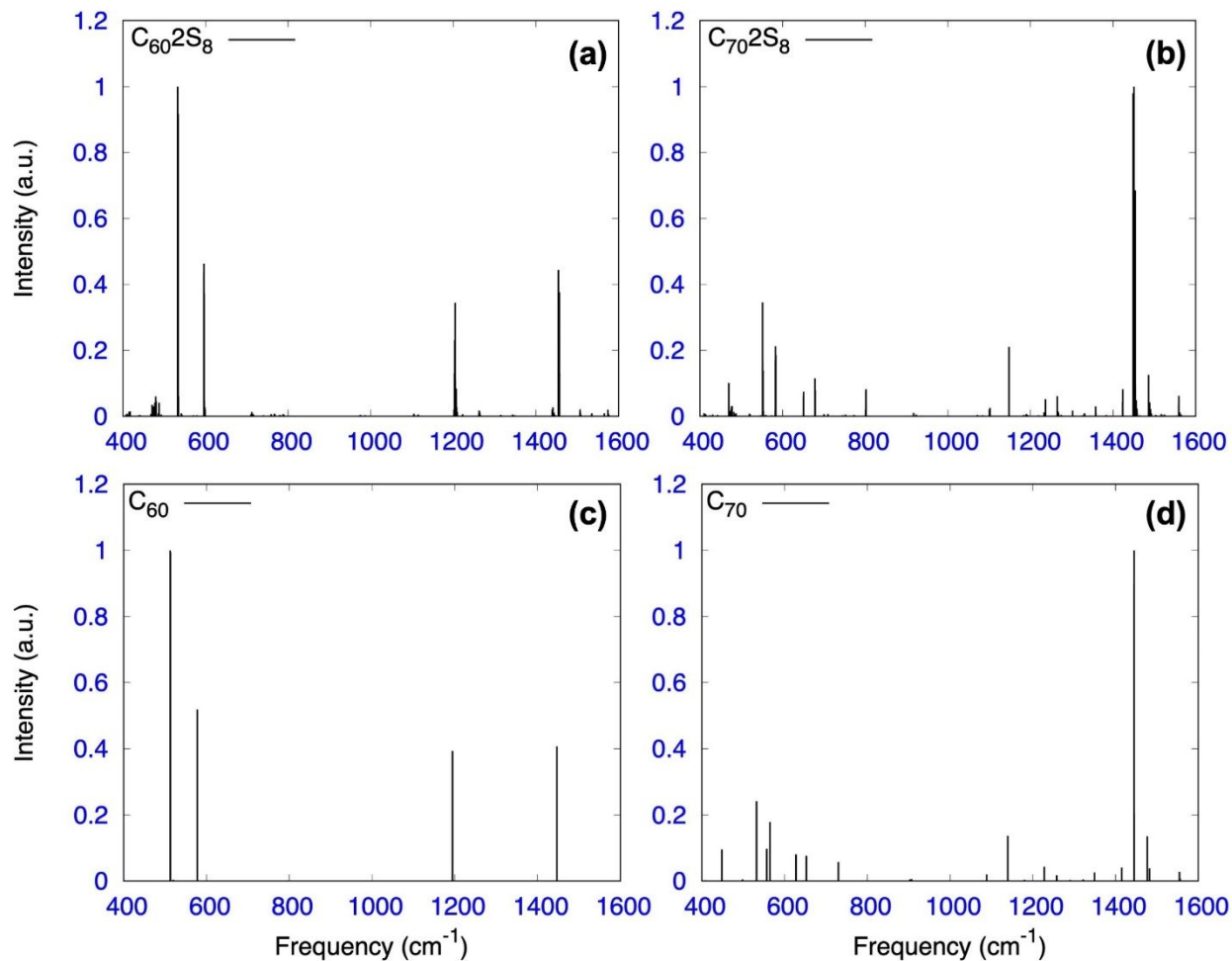


Figure 3. IR spectra of the C₆₀-2S₈ (a) and C₇₀-2S₈ (b) co-crystals and IR spectra of isolated C₆₀ (c) and C₇₀ (d) molecules, as calculated at the PBE level.

Optical properties. We now turn to the optical properties of the C₆₀-2S₈ and C₇₀-2S₈ co-crystals.

Here, in order to estimate the lowest excited-state energies of the systems, we performed TD-DFT calculations at the B3LYP/6-31G (d,p) level based on fullerene-S₈ complexes extracted from the crystal structures and consisting of one fullerene molecule and one S₈ molecule. The calculated transition energies of the lowest singlet states of the C₆₀-S₈ and C₇₀-S₈ complexes are presented in

Table S4; selected transitions of interest in the $C_{60} - S_8$ complex along with the transition energies in the isolated molecules are also collected also in **Table 3**.

Table 3. Singlet excited-state transition energies (in eV) of the S_8 and C_{60} molecules and S_8-C_{60} complex, as obtained from TD-DFT calculations at the B3LYP/6-31G (d,p) level of theory.

Transition	S_8	C_{60}	S_8-C_{60}
$S_0 \rightarrow S_1$	3.73	2.10	2.09
.....
$S_0 \rightarrow S_{15}$	4.30	2.28	2.28
$S_0 \rightarrow S_{16}$	4.34	3.21	2.84

The TD-DFT/B3LYP results highlight that the energies of the lowest 15 excited states of $C_{60}-S_8$ are identical to those of C_{60} itself. However, the energy of the next ($S_0 \rightarrow S_{16}$) transition in the complex is lower than the corresponding transition in C_{60} and the energy of the first excited state of S_8 . This clearly indicates that the S_{16} excited state in the complex is due to interactions between C_{60} and S_8 molecules. The natural transition orbitals shown in **Figure 4** indeed point to the $S_0 \rightarrow S_{16}$ transition in the co-crystal as representing a charge-transfer transition with an electron being transferred from C_{60} to S_8 . A similar situation is found for the $C_{70} - 2S_8$ co-crystal, see **Table S4** and **Figure S4**. Thus, in both co-crystals, the lowest excited states are dominated by transitions localized on the fullerene molecules. A similar nature of the CT states is also obtained by means of TD-DFT LC- ω HPBE calculations (see **Figure S5** and **Table S5**). This finding is supported by the experimental data showing that the optical spectra of the co-crystals are similar to those of the pure fullerenes and exhibit just an additional marginal transition above the optical edge of the fullerene bands.⁷⁹

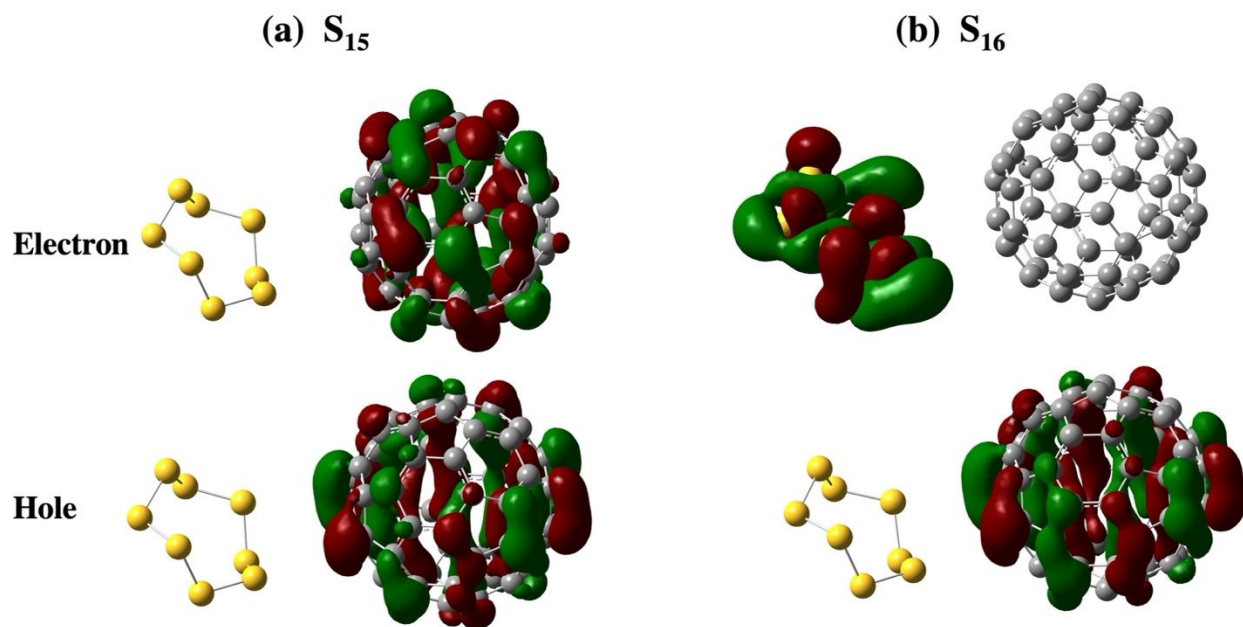


Figure 4. Comparison of the B3LYP/6-31G (d,p) natural transition orbitals (NTOs) in the $C_{60} - S_8$ complex between (a) the C_{60} singlet local excited state S_{15} (λ value for the NTO shown is 0.67; the other relevant NTOs involve additional fullerene frontier molecular orbitals) and (b) the lowest singlet charge-transfer state ($\lambda(\text{NTO}) = 0.99$), *i.e.*, the S_{16} state.

4. Conclusions

We performed DFT calculations to investigate the charge transport, vibrational, and optical properties of the $C_{60} - 2S_8$ and $C_{70} - 2S_8$ co-crystals. DFT calculations on the crystals, fullerene- S_8 complexes, and the individual molecules demonstrate that all these properties are dominated by the fullerene component.

With regard to charge transport, the presence of the S_8 molecules does not contribute to, but also does not affect the properties of both holes and electrons in the co-crystals, with transport taking place over the networks of fullerene molecules. Interestingly, small effective masses are found for

holes and electrons in both co-crystals with transport displaying a 3D character in the case of electrons.

Our calculations also show that there exist only weak van der Waals interactions between the fullerene and S_8 molecules in both co-crystals; in agreement with experimental data, the calculated IR spectra of the co-crystals essentially represent a simple superposition of the individual spectra of S_8 and fullerene molecules. Our results also suggest that fullerene- S_8 co-crystals could be potential candidates for thermal LWIR and MWIR imaging applications.

In terms of the optical properties, it is found that the charge-transfer transitions in both $C_{60}-2S_8$ and $C_{70}-2S_8$ co-crystals are located above the lowest excited states of the fullerenes. Thus, given that the first excited state in the S_8 molecule has a very high energy, the low-energy part of the optical spectra in the fullerene- S_8 co-crystals are dominated by transitions within the fullerene component.

Finally, our results indicate that, due its optical transparency over a large energy window and the simplicity of its vibrational spectrum, an S_8 matrix could be used to test the effect of a solid-state environment on the intramolecular properties of various molecules and molecular complexes.

5. Acknowledgements

This work was funded by the National Science Foundation and the Air Force Research Laboratory through DMREF-2118578 and by the College of Science of the University of Arizona. The authors are thankful for the use of the High Performance Computing (HPC) resources supported by the

University of Arizona TRIF, UITS, and Research, Innovation, and Impact (RII) Offices and maintained by the Research Technologies Department.

References

1. Kleine, T. S.; Glass, R. S.; Lichtenberger, D. L.; Mackay, M. E.; Char, K.; Norwood, R. A.; Pyun, J., 100th Anniversary of Macromolecular Science Viewpoint: High Refractive Index Polymers from Elemental Sulfur for Infrared Thermal Imaging and Optics. *ACS Macro Letters* **2020**, *9* (2), 245-259.
2. Griebel, J. J.; Namnabat, S.; Kim, E. T.; Himmelhuber, R.; Moronta, D. H.; Chung, W. J.; Simmonds, A. G.; Kim, K. J.; Van Der Laan, J.; Nguyen, N. A., New infrared transmitting material via inverse vulcanization of elemental sulfur to prepare high refractive index polymers. *Advanced Materials* **2014**, *26* (19), 3014-3018.
3. Dirlam, P. T.; Park, J.; Simmonds, A. G.; Domanik, K.; Arrington, C. B.; Schaefer, J. L.; Oleshko, V. P.; Kleine, T. S.; Char, K.; Glass, R. S., Elemental sulfur and molybdenum disulfide composites for Li-S batteries with long cycle life and high-rate capability. *ACS Applied Materials & Interfaces* **2016**, *8* (21), 13437-13448.
4. Ji, X.; Lee, K. T.; Nazar, L. F., A highly ordered nanostructured carbon-sulphur cathode for lithium-sulphur batteries. *Nature materials* **2009**, *8* (6), 500-506.
5. Wang, D.; Tang, Z.; Huang, R.; Duan, Y.; Wu, S.; Guo, B.; Zhang, L., Interface Coupling in Rubber/Carbon Black Composites toward Superior Energy-Saving Capability Enabled by Amino-Functionalized Polysulfide. *Chemistry of Materials* **2022**, *35* (2), 764-772.
6. Tonkin, S. J.; Gibson, C. T.; Campbell, J. A.; Lewis, D. A.; Karton, A.; Hasell, T.; Chalker, J. M., Chemically induced repair, adhesion, and recycling of polymers made by inverse vulcanization. *Chemical Science* **2020**, *11* (21), 5537-5546.
7. Yue, T.-J.; Wang, L.-Y.; Ren, W.-M., The synthesis of degradable sulfur-containing polymers: precise control of structure and stereochemistry. *Polymer Chemistry* **2021**, *12* (46), 6650-6666.
8. Mann, M.; Zhang, B.; Tonkin, S. J.; Gibson, C. T.; Jia, Z.; Hasell, T.; Chalker, J. M., Processes for coating surfaces with a copolymer made from sulfur and dicyclopentadiene. *Polymer Chemistry* **2022**, *13* (10), 1320-1327.
9. Mann, M.; Kruger, J. E.; Andari, F.; McErlean, J.; Gascooke, J. R.; Smith, J. A.; Worthington, M. J.; McKinley, C. C.; Campbell, J. A.; Lewis, D. A., Sulfur polymer composites as controlled-release fertilisers. *Organic & biomolecular chemistry* **2019**, *17* (7), 1929-1936.
10. Chalker, J. M.; Mann, M.; Worthington, M. J.; Esdaile, L. J., Polymers made by inverse vulcanization for use as mercury sorbents. *Organic Materials* **2021**, *3* (02), 362-373.
11. Lim, J.; Pyun, J.; Char, K., Recent approaches for the direct use of elemental sulfur in the synthesis and processing of advanced materials. *Angewandte Chemie International Edition* **2015**, *54* (11), 3249-3258.

12. Chung, W. J.; Griebel, J. J.; Kim, E. T.; Yoon, H.; Simmonds, A. G.; Ji, H. J.; Dirlam, P. T.; Glass, R. S.; Wie, J. J.; Nguyen, N. A., The use of elemental sulfur as an alternative feedstock for polymeric materials. *Nature chemistry* **2013**, *5* (6), 518-524.
13. Steudel, R., Liquid Sulfur. *Top. Curr. Chem.* **2003**, *230*, 81-116.
14. Liu, L.; Kono, Y.; Kenney-Benson, C.; Yang, W.; Bi, Y.; Shen, G., Chain Breakage in Liquid Sulfur at High Pressures and High Temperatures. *Physical Review B* **2014**, *89* (17), 174201.
15. Zhang, L.; Ren, Y.; Liu, X.; Han, F.; Evans-Lutterodt, K.; Wang, H.; He, Y.; Wang, J.; Zhao, Y.; Yang, W., Chain Breakage in the Supercooled Liquid - Liquid Transition and Re-entry of the λ -transition in Sulfur. *Sci Rep* **2018**, *8* (1), 4558-4558.
16. Henry, L.; Mezouar, M.; Garbarino, G.; Sifré, D.; Weck, G.; Datchi, F., Liquid-Liquid Transition and Critical Point in Sulfur. *Nature* **2020**, *584* (7821), 382-386.
17. Powell, R. E.; Eyring, H., The Properties of Liquid Sulfur. *Journal of the American Chemical Society* **1943**, *65* (4), 648-654.
18. Schmidt, M., Elemental Sulfur-A Challenge to Theory and Practice. *Angewandte Chemie International Edition in English* **1973**, *12* (6), 445-455.
19. Meyer, B., Elemental Sulfur. *Chem. Rev.* **1976**, *76* (3), 367-388.
20. Steudel, R.; Eckert, B.; Steudel, Y.; Wong, M. W., Elemental Sulfur and Sulfur-Rich Compounds I. *Top. Curr. Chem.* **2003**, *230*, 1-134.
21. Meyer, B.; Gouterman, M.; Jensen, D.; Oommen, T.; Spitzer, K.; Stroyer-Hansen, T., The spectrum of sulfur and its allotropes. ACS Publications: 1972.
22. Abrahams, S. C., The crystal and molecular structure of orthorhombic sulfur. *Acta Crystallographica* **1955**, *8* (11), 661-671.
23. Hao, M.-T.; Du, C.-F.; Tian, C.-B.; Li, J.-R.; Huang, X.-Y., [Fe (SCN) 2 (bipy) 2] · 2 (S8): A two-dimensional coordination polymer intercalating the S8 molecules. *Inorganic Chemistry Communications* **2016**, *72*, 128-131.
24. Cotton, F. A.; Kibala, P. A.; Sandor, R. B., Structural characterization of WCl6 · S8. *Acta Crystallographica Section C: Crystal Structure Communications* **1989**, *45* (9), 1287-1289.
25. Ghiassi, K. B.; Chen, S. Y.; Wescott, J.; Balch, A. L.; Olmstead, M. M., New insights into the structural complexity of C60 · 2S8: Two crystal morphologies, two phase changes, four polymorphs. *Crystal Growth & Design* **2015**, *15* (1), 404-410.
26. Allouchi, H.; López, D. O.; Gardette, M. F.; Tamarit, J. L.; Agafonov, V.; Szwarc, H.; Céolin, R., Thermal and mechanical behaviour of the C60 · 2S8 monoclinic compound. *Chemical Physics Letters* **2000**, *317* (1-2), 40-44.

27. Baratta, W.; Calderazzo, F.; Daniels, L. M., cyclo-Octasulfur Adducts of $\text{WCl}_4(\text{S})(\text{THF})$ and WCl_6 . Crystal and Molecular Structure of $\text{WCl}_4(\text{S})(\text{THF}) \cdot \text{S}_8$. *Inorganic Chemistry* **1994**, *33* (17), 3842-3844.
28. Bjorvatten, T.; Hassel, O.; Lindheim, A., Crystal Structure of the Addition Compound $\text{SbI}_3 \cdot 3\text{S}_8$. *Acta Chem. Scand.* **1963**, *17*.
29. Buravov, L. I.; D'Yachenko, O. A.; Konovalikhin, S. V.; Kushch, N. D.; Lavrent'ev, I. P.; Spitsyna, N. G.; Shilov, G. V.; Yagubskii, E. B., A complex of buckminsterfullerene with sulfur, $\text{C}_{60} \cdot 2\text{S}_8$: synthesis and crystal structure. *Russian Chemical Bulletin* **1994**, *43* (2), 240-244.
30. Cotton, F. A.; Kibala, P. A.; Sandor, R. B. W., Structural Characterization of $\text{WCl}_6 \cdot \text{S}_8$. *Acta Crystallogr.* **1989**.
31. Fernando, W. S., Single crystal Raman spectra of $\text{SbI}_3 \cdot 3\text{S}_8$; $\text{CHI}_3 \cdot 3\text{S}_8$ and $\text{AsI}_3 \cdot 3\text{S}_8$. *Journal of Inorganic and Nuclear Chemistry* **1981**, *43* (6), 1141-1145.
32. Ghiassi, K. B.; Chen, S. Y.; Wescott, J.; Balch, A. L.; Olmstead, M. M., New insights into the structural complexity of $\text{C}_{60} \cdot 2\text{S}_8$: Two crystal morphologies, two phase changes, four polymorphs. *Crystal Growth and Design* **2015**, *15* (1), 404-410a.
33. Kelly, J. F.; Samoc, A.; Samoc, M.; Krausz, E. R.; Willis, A. C., Anisotropy of second-order nonlinear optical susceptibilities of arsenic triiodide-sulfur addition complex: $\text{AsI}_3 \cdot 3\text{S}_8$. *Optics Communications* **2006**, *264* (1), 35-44.
34. Laitinen, R.; Steidel, J.; Steudel, R., The Crystal Structures and Raman Spectra of $2\text{S}_8 \cdot \text{SnI}_4$ and $2\text{S}(n)\text{Se}(8-n) \cdot \text{SnI}_4$. *Acta Chemica Scandinavica* **1980**, *34 A*.
35. Marking, G. A.; Kanatzidis, M. G., Encapsulation of Cyclooctasulfur Molecules in an Open Metal-Sulfide Framework. Isolation of the Host-Guest Complex $\text{Cs}_2\text{Sn}_3\text{S}_7 \cdot 1/2\text{S}_8$ from Molten Cesium Polysulfide Fluxes. *Chemistry of Materials* **1995**, *7* (10), 1915-1921.
36. Michel, R. H.; Kappes, M. M.; Adelman, P.; Roth, G., Preparation and Structure of $\text{C}_{76}(\text{S}_8)_6$: A First Step in the Crystallographic Investigation of Higher Fullerenes. *Angewandte Chemie International Edition in English* **1994**, *33* (15-16), 1651-1654.
37. Kroto, H. W.; Heath, J. R.; O'Brien, S. C.; Curl, R. F.; Smalley, R. E., C_{60} : Buckminsterfullerene. *Nature* **1985**, *318* (6042), 162-163.
38. Haddon, R. C.; Hebard, A. F.; Rosseinsky, M. J.; Murphy, D. W.; Duclos, S. J.; Lyons, K. B.; Miller, B.; Rosamilia, J. M.; Fleming, R. M.; Kortan, A. R.; Glarum, S. H.; Makhija, A. V.; Muller, A. J.; Eick, R. H.; Zahurak, S. M.; Tycko, R.; Dabbagh, G.; Thiel, F. A., Conducting Films of C_{60} and C_{70} by Alkali-Metal Doping. *Nature* **1991**, *350* (6316), 320-322.
39. Sathiyamoorthy, V. N.; Mizuseki, H.; Kawazoe, Y., Hydrogen Storage on Nanofullerene Cages. *Nano* **2009**, *04* (05), 253-263.

40. Han, S. S.; Mendoza-Cortés, J. L.; Goddard III, W. A., Recent Advances on Simulation and Theory of Hydrogen Storage in Metal–Organic Frameworks and Covalent Organic Frameworks. *Chemical Society Reviews* **2009**, *38* (5), 1460-1476.
41. Goodarzi, S.; Da Ros, T.; Conde, J.; Sefat, F.; Mozafari, M., Fullerene: Biomedical Engineers Get to Revisit an Old Friend. *Materials Today* **2017**, *20* (8), 460-480.
42. Yin, H.; Lin, H.; Zong, Y.; Wang, X.-D., The Recent Advances in C60 Micro/Nanostructures and their Optoelectronic Applications. *Organic Electronics* **2021**, *93*, 106142.
43. Makha, M.; Purich, A.; Raston, C. L.; Sobolev, A. N., Structural diversity of host–guest and intercalation complexes of fullerene C60. *European journal of inorganic chemistry* **2006**, *2006* (3), 507-517.
44. Yang, J.; Sullivan, P.; Schumann, S.; Hancox, I.; Jones, T. S., Organic photovoltaic cells based on unconventional electron donor fullerene and electron acceptor copper hexadecafluorophthalocyanine. *Applied physics letters* **2012**, *100* (2).
45. Zhuang, T.; Wang, X.-F.; Sano, T.; Hong, Z.; Li, G.; Yang, Y.; Kido, J., Fullerene C70 as a p-type donor in organic photovoltaic cells. *Applied Physics Letters* **2014**, *105* (9).
46. Xing, Z.; Liu, F.; Li, S. H.; Huang, X.; Fan, A.; Huang, Q.; Yang, S., Bowl-Assisted Ball Assembly for Solvent-Processing the C60 Electron Transport Layer of High-Performance Inverted Perovskite Solar Cell. *Angewandte Chemie International Edition* **2023**, *62* (34), e202305357.
47. Wetzelaer, G., Trap-free space-charge-limited hole transport in a fullerene derivative. *Physical Review Applied* **2019**, *11* (2), 024069.
48. Ambipolar organic field-effect transistors based on a solution-processed methanofullerene. *Advanced Materials* **2004**, *16* (23-24), 2174-2179.
49. Cho, E.; Coropceanu, V.; Brédas, J.-L., Hole versus electron transport in fullerenes. *Organic Electronics* **2023**, *118*, 106798.
50. Gong, J.; Li, Y.; Lin, S.; Ma, G.; Yang, Y.; Chen, G., Enhancement of electrical conductivity in sulfur-doped C60 films. *Thin Solid Films* **1997**, *302* (1), 256-259.
51. Allouchi, H.; López, D.; Gardette, M.-F.; Tamarit, J. L.; Agafonov, V.; Szwarc, H.; Céolin, R., Thermal and mechanical behaviour of the C60·2S8 monoclinic compound. *Chemical Physics Letters* **2000**, *317* (1-2), 40-44.
52. Takahashi, H.; Matsubara, E.; Shiro, M.; Matsubara, S.; Sato, N.; Muramatsu, A.; Tohji, K., Co-deposition of fullerenes and sulfur from diluted solution. *Fullerenes, Nanotubes and Carbon Nanostructures* **2002**, *10* (3), 217-226.
53. Roth, G.; Adelman, P., Preparation and crystal structure of C 60 S 16. *Applied Physics A* **1993**, *56*, 169-174.

54. Michel, R. H.; Kappes, M. M.; Adelman, P.; Roth, G., Preparation and structure of C₇₆ (S₈)₆: A first step in the crystallographic investigation of higher fullerenes. *Angewandte Chemie International Edition in English* **1994**, *33* (15-16), 1651-1654.
55. Grell, A.-S.; Masin, F.; Céolin, R.; Gardette, M. F.; Szwarc, H., Molecular dynamics of C₆₀·2 S₈: A ¹³C NMR study. *Physical Review B* **2000**, *62* (6), 3722.
56. Gardette, M.-F.; Chilouet, A.; Toscani, S.; Allouchi, H.; Agafonov, V.; Rouland, J.-C.; Szwarc, H.; Céolin, R., Phase equilibria in the C₆₀–sulphur system. *Chemical physics letters* **1999**, *306* (3-4), 149-154.
57. Talyzin, A. V.; Tergenius, L. E.; Jansson, U., Single-crystal growth of C₇₀S₈ – a new phase in the C₇₀–sulphur system. *Journal of Crystal Growth* **2000**, *213* (1), 63-69.
58. Talyzin, A.; Jansson, U., Preparation and characterization of C₆₀S₁₆ and C₇₀S₄₈ thin films. *Thin Solid Films* **1999**, *350* (1-2), 113-118.
59. Takahashi, H.; Matsubara, E.; Belosludov, R.; Vladimirovich; Matsubara, S.; Sato, N.; Muramatsu, A.; Kawazoe, Y.; Tohji, K., Fullerene and Sulfur Compounds. *MATERIALS TRANSACTIONS* **2002**, *43* (7), 1530-1532.
60. Xiang, J.; Shen, W.; Guo, Z.; Meng, J.; Yuan, L.; Zhang, Y.; Cheng, Z.; Shen, Y.; Lu, X.; Huang, Y., A Supramolecular Complex of C₆₀–S with High-Density Active Sites as a Cathode for Lithium–Sulfur Batteries. *Angewandte Chemie International Edition* **2021**, *60* (26), 14313-14318.
61. Wang, L., Solvated fullerenes, a new class of carbon materials suitable for high-pressure studies: A review. *Journal of Physics and Chemistry of Solids* **2015**, *84*, 85-95.
62. Hafner, J., Ab-initio simulations of materials using VASP: Density-functional theory and beyond. *Journal of computational chemistry* **2008**, *29* (13), 2044-2078.
63. Perdew, J. P.; Burke, K.; Ernzerhof, M., Generalized gradient approximation made simple. *Physical review letters* **1996**, *77* (18), 3865.
64. Kresse, G.; Furthmüller, J., Efficient iterative schemes for ab initio total-energy calculations using a plane-wave basis set. *Physical review B* **1996**, *54* (16), 11169.
65. Wu, X.; Vanderbilt, D.; Hamann, D., Systematic treatment of displacements, strains, and electric fields in density-functional perturbation theory. *Physical Review B* **2005**, *72* (3), 035105.
66. Karhanek, D., *Self-assembled monolayers studied by density-functional theory*. na: 2010.
67. Valeev, E. F.; Coropceanu, V.; da Silva Filho, D. A.; Salman, S.; Brédas, J.-L., Effect of Electronic Polarization on Charge-Transport Parameters in Molecular Organic Semiconductors. *Journal of the American Chemical Society* **2006**, *128* (30), 9882-9886.

68. Yi, Y.; Coropceanu, V.; Brédas, J.-L., Nonlocal Electron-Phonon Coupling in the Pentacene Crystal: Beyond the Γ -Point Approximation. *The Journal of Chemical Physics* **2012**, *137* (16), 164303.
69. Cho, E.; Coropceanu, V.; Brédas, J.-L., Electronic Structure of Multicomponent Organic Molecular Materials: Evaluation of Range-Separated Hybrid Functionals. *Journal of Chemical Theory and Computation* **2020**, *16* (6), 3712-3719.
70. Donaldson, A.; Caplin, A., Refractive index of molten sulphur. *Philosophical Magazine B* **1985**, *52* (2), 185-197.
71. Sami, S.; Haase, P. A.; Alessandri, R.; Broer, R.; Havenith, R. W., Can the dielectric constant of fullerene derivatives be enhanced by side-chain manipulation? A predictive first-principles computational study. *The Journal of Physical Chemistry A* **2018**, *122* (15), 3919-3926.
72. Frisch, M.; Trucks, G.; Schlegel, H. B.; Scuseria, G.; Robb, M.; Cheeseman, J.; Scalmani, G.; Barone, V.; Petersson, G.; Nakatsuji, H., Gaussian 16. Gaussian, Inc. Wallingford, CT: 2016.
73. Saito, S.; Oshiyama, A., Cohesive mechanism and energy bands of solid C_{60} . *Physical Review Letters* **1991**, *66* (20), 2637-2640.
74. Chung, W. J.; Griebel, J. J.; Kim, E. T.; Yoon, H.; Simmonds, A. G.; Ji, H. J.; Dirlam, P. T.; Glass, R. S.; Wie, J. J.; Nguyen, N. A.; Guralnick, B. W.; Park, J.; Somogyi, Á.; Theato, P.; Mackay, M. E.; Sung, Y.-E.; Char, K.; Pyun, J., The Use of Elemental Sulfur as an Alternative Feedstock for Polymeric Materials. *Nature Chemistry* **2013**, *5* (6), 518-524.
75. Griebel, J. J.; Namnabat, S.; Kim, E. T.; Himmelhuber, R.; Moronta, D. H.; Chung, W. J.; Simmonds, A. G.; Kim, K.-J.; van der Laan, J.; Nguyen, N. A.; Dereniak, E. L.; Mackay, M. E.; Char, K.; Glass, R. S.; Norwood, R. A.; Pyun, J., New Infrared Transmitting Material via Inverse Vulcanization of Elemental Sulfur to Prepare High Refractive Index Polymers. *Advanced Materials* **2014**, *26* (19), 3014-3018.
76. Lee, T.; Dirlam, P. T.; Njardarson, J. T.; Glass, R. S.; Pyun, J., Polymerizations with Elemental Sulfur: From Petroleum Refining to Polymeric Materials. *Journal of the American Chemical Society* **2022**, *144* (1), 5-22.
77. Steudel, R., *Elemental sulfur and sulfur-rich compounds II*. Springer Science & Business Media: 2003; Vol. 2.
78. Cho, E.; Pratik, S. M.; Pyun, J.; Coropceanu, V.; Brédas, J.-L., π -Conjugated Carbon-Based Materials for Infrared Thermal Imaging. *Advanced Optical Materials* **2023**, *11* (12), 2300029.
79. Kushch, N. D.; Majchrzak, I.; Ciesielski, W.; Graja, A.; Woźniak, K.; Krygowski, T. M., New sulfur-fullerite; its preparation, structure and spectral properties. *J. Phys. I France* **1993**, *3* (10), 1987-1991.